JOURNAL OF APPLIED ELECTROCHEMISTRY 16 (1986) 643–653

Process modelling in the porous molten carbonate fuel cell (MCFC) cathode

J. JEWULSKI*

Polish Academy of Sciences, Institute of Physical Chemistry, Molten Salts Laboratory, al. Mickiewicza 30, PL-30-059 Kraków, Poland

Received 8 October 1984; revised 19 July 1985

An isotropic, one-dimensional, complex model of the porous NiO cathode for a molten carbonate fuel cell (MCFC) is considered with the general assumptions as previously described for the MCFC anode. A reaction mechanism for the NiO cathode is proposed and discussed as well as 'effective' quantities in the porous electrode. Gas phase transport limitations of reagents are discussed on the basis of the 'dusty gas' model. The model equations are solved numerically for half-cell polarizations and the results are in good agreement with different experimental investigations.

Nomenclature

a_i^{eff}	effective reaction order (in the porous electrode)
B_0	permeability factor
c_k	molar concentration of the kth component at the electrode–electrolyte interface
c_k^0	equilibrium molar concentration of the kth gas component in the electrolyte
D_k	diffusion coefficient of the kth component in the electrolyte
$D_{K,k}$	Knudsen diffusion coefficient
D_{ij}	binary diffusion coefficient
F	Faraday's constant
H_k	Henry's constant of the kth gas component
i_0	exchange current density
i_0^0	standard current density
i_k^{lim}	limiting current density of the kth component
i	Faradiac current density
j	current density
j_T	total current density
k	rate constant in Equation 13
K_0	'diffusion attenuation coefficient' in the porous structure
l	electrode thickness
M_k	molecular weight of the kth component
n	number of electrons transferred (in the overall stoichiometric equation)
N_k	molar flux of the kth gas component
p_k	partial pressure of the kth component
p_k^0	partial pressure of the kth component at $x = 0$
p	total pressure
R	gas constant
s	parameter defined by Equation 24
S	specific internal surface of the porous electrode, electrochemically active
T	temperature
x	coordinate (gas–porous electrode interface, $x = 0$, porous electrode–separator interface, $x = l$)
Z	total resistance of the porous electrode
ΔV_{IR}	ohmic loss
α	transfer coefficient
δ	electrolyte film thickness
ε	porosity
η	local overpotential
η_m	measured overpotential
η_N	concentration overpotential in the gas phase (Nernst loss)
κ^{eff}	effective specific conductivity
ν	stoichiometric number
ν_k	stoichiometric coefficient of the kth component (in the overall stoichiometric equation)
μ	gas mixture viscosity

* *Present address*: Institute of Computer Science, AGH, al Mickiewicza 30, PL-30-059 Kraków, Poland.

Subscripts

a anodic
c cathodic
eff effective (apparent)
E electrolyte
M electrode material

1. Introduction

In the previous paper [1] a model of the isotropic molten carbonate fuel cell (MCFC) anode was proposed and discussed against a background of other models. The aim of this paper is to apply that model to the process modelling in the porous MCFC cathode (under the same general assumptions). The thin film anisotropic model [2–4] and the agglomerate model [5, 6] have already been considered in respect to that problem.

The knowledge of the mechanism of the overall cathodic reaction

$$\tfrac{1}{2}O_2 + CO_2 + 2e \rightleftharpoons CO_3^{2-} \tag{1}$$

is fundamental for the mathematical description of microscopic processes. It allows us to derive the generalized Butler–Volmer-type equation on the basis of the rate-determining step concept. Unfortunately, up until now, there have been no experimental results on the flat NiO cathode which could be used to deduce the reaction mechanism. Hitherto, the description of the mechanism has been related to flat gold cathodes [7, 8] or, in the case of the NiO cathodes, it is speculative [5]. In this paper, data obtained on the porous NiO cathode [9, 10] and theoretical considerations of the porous electrode behaviour as a function of its microscopic and macroscopic parameters are used to propose the mechanism of the cathode reaction.

With regard to macroscopic processes, the paper presents an extended version of the thin film isotropic model. In addition, it considers the influence of the gas phase multicomponent transport limitations on the electrochemical activity of the porous NiO cathode. This problem has not been studied in detail until now, previous work being limited to simple estimations [11, 12] or imprecise descriptions.

2. Theory

2.1. *Total impedance of the porous electrode*

The basic equation which describes the behaviour of the porous electrode in the isotropic model can be written

$$\frac{d^2\eta}{dx^2} = S\left(\frac{1}{\kappa_E^{eff}} + \frac{1}{\kappa_M^{eff}}\right) i(\eta) \tag{2}$$

with boundary conditions

$$\left.\frac{d\eta}{dx}\right|_{x=0} = -j_T/\kappa_M^{eff} \tag{3}$$

$$\left.\frac{d\eta}{dx}\right|_{x=l} = j_T/\kappa_E^{eff} \tag{4}$$

This equation can be analytically solved only in special cases, among which an interesting case represents the linear relationship of the generated Faradic current density and local overpotential:

$$\eta = Z_F i \tag{5}$$

In this case, the solution for the total electrode impedance has a form

$$Z = \frac{\cosh(l/l_{\text{eff}})[1 + (\kappa_{\text{E}}^{\text{eff}}/\kappa_{\text{M}}^{\text{eff}})^2] + 2\kappa_{\text{E}}^{\text{eff}}/\kappa_{\text{M}}^{\text{eff}}}{\sinh(l/l_{\text{eff}})\kappa_{\text{E}}^{\text{eff}}(1 + \kappa_{\text{E}}^{\text{eff}}/\kappa_{\text{M}}^{\text{eff}})} l_{\text{eff}} + \frac{1}{\kappa_{\text{M}}^{\text{eff}}(1 + \kappa_{\text{E}}^{\text{eff}}/\kappa_{\text{M}}^{\text{eff}})} \tag{6}$$

where

$$l_{\text{eff}} = \left[\frac{S}{Z_{\text{F}}}\left(\frac{1}{\kappa_{\text{E}}^{\text{eff}}} + \frac{1}{\kappa_{\text{M}}^{\text{eff}}}\right)\right]^{-0.5} \tag{7}$$

Z_{F} is the microscopic internal resistance of the inner, electrochemically active surface of the electrode. It can be represented as a sum of the activation resistance, Z^{act} (resulting from the finite rate of the electrode reaction), and of the diffusion resistances, $Z_{\text{j}}^{\text{dif}}$ (resulting from limitations of the jth reagent transport through the electrolyte) [13]:

$$Z_{\text{F}} = Z^{\text{act}} + \sum_{j=1}^{N} Z_{\text{j}}^{\text{dif}} \tag{8}$$

where

$$Z^{\text{act}} = \frac{RTv}{nFi_0} \tag{9}$$

$$Z_{\text{j}}^{\text{dif}} = \frac{RTv_j}{nFi_{\text{j}}^{\text{lim}}} \tag{10}$$

Experimentally measured specific effective solid phase conductivity of the porous NiO cathode (lithiated and oxidized *in situ*, porosity about 60%) is $\kappa_{\text{M}}^{\text{eff}} = 8\,\Omega^{-1}\,\text{cm}^{-1}$ at 923 K [14]. In this case the ohmic losses in the solid phase can be neglected for a typical MCFC cathode thickness (0.05–0.10 cm), and Equation 6 becomes simplified to

$$j_{\text{T}} = \left(\frac{S\kappa_{\text{E}}^{\text{eff}}}{Z_{\text{F}}}\right)^{0.5} \tanh\left[\left(\frac{S}{Z_{\text{F}}\kappa_{\text{E}}^{\text{eff}}}\right)^{0.5} l\right]\eta_{\text{m}} \tag{11}$$

For other materials applicable as porous MCFC cathodes, e.g. CuO ($\kappa_{\text{M}}^{\text{eff}} = 0.23\,\Omega^{-1}\,\text{cm}^{-1}$ [15]), the full form of Equation 6 could be taken into consideration.

2.2. *Effective exchange current density*

Because of the lack of experimental data on the flat NiO cathode, results of investigations of the effective exchange current on porous NiO cathodes were used in order to determine the reaction mechanism. On the basis of analogy with the flat electrode, the dependence of the total current density on the overpotential may be expressed for the porous electrode as

$$j_{\text{T}} = i_0^{\text{eff}}\left(\exp\frac{\alpha_{\text{a}}^{\text{eff}}F\eta}{RT} - \exp\frac{-\alpha_{\text{c}}^{\text{eff}}F\eta}{RT}\right) \tag{12}$$

where

$$i_0^{\text{eff}} = k\prod_{j=1}^{N}(p_{\text{j}})^{a_{\text{j}}^{\text{eff}}} \tag{13}$$

The reaction order of the effective exchange current defined as

$$a_{\text{i}}^{\text{eff}} = \left.\frac{\partial \ln i_0^{\text{eff}}}{\partial \ln p_{\text{i}}}\right|_{p_{j\neq i}} = \left.\frac{\partial \ln j_{\text{T}}}{\partial \ln p_{\text{i}}}\right|_{p_{j\neq i},\eta} \tag{14}$$

is the complex function of the microkinetic and macrokinetic parameters of the porous electrode.

Table 1. Possible regions of the porous electrode operation

Conditions of the porous electrode operations			
Macrokinetic		*Microkinetic*	
$l_{eff} \gg 1$ 'Thin electrode'–negligible ohmic losses inside the porous electrode	$l_{eff} \ll 1$ 'Thick electrode'–ohmic control of the porous electrode operation	$Z^{act} \gg Z_i^{dif}$ $(i = 1, \ldots, N)$ Activation control condition	$\Sigma_{i=1}^{N} Z_i^{dif} \gg Z^{act}$ Diffusion control condition
$f_{macro} = 1.0$	$f_{macro} = 0.5$	$f_{micro}^{i} = a_i$	$f_{micro}^{i} = \Sigma_j a_{ij}^{dif} Z_j^{dif}/Z_F$
$0.5 f_{micro}^{i} \leqslant a_i^{eff} \leqslant f_{micro}^{i}$		$0.5 a_i \leqslant a_i^{eff} \leqslant a_i$	$0.5 a_{ij_0}^{dif} \leqslant a_i^{eff} \leqslant a_{ij_0}^{dif}$ if $Z_{j_0}^{dif} \gg Z_j^{dif}$ at $j \neq j_0$

We define

$$a_i = \left.\frac{\partial \ln i_0}{\partial \ln p_i}\right|_{p_{j\neq i}} \tag{15}$$

and

$$a_{ij}^{dif} = \left.\frac{\partial \ln i_j^{lim}}{\partial \ln p_i}\right|_{p_{j\neq i}} \tag{16}$$

Using Equations 11 and 14–16 yields

$$a_i^{eff} = f_{micro}^{i} f_{macro} \tag{17}$$

where

$$f_{micro}^{i} = \frac{a_i Z^{act} + \sum_{j=1}^{N} a_{ij}^{dif} Z_j^{dif}}{Z_F} \tag{18}$$

$$f_{macro} = 0.5 + \frac{l/l_{eff}}{\sinh(2l/l_{eff})} \tag{19}$$

Equation 17 permits us to determine the influence of the basic microscopic and macroscopic parameters on the observed effective exchange current in the porous electrode. The possible regions of the porous electrode operation are summarized in Table 1. It is easy to show that, according to the macroscopic region in which the porous electrode operates, orders of the effective exchange current can vary within the interval

$$0.5 f_{micro}^{i} \leqslant a_i^{eff} \leqslant f_{micro}^{i} \tag{20}$$

In order to calculate the f_{micro}^{i} factor, the reaction orders a_i of the 'true' exchange current are needed, as well as the a_{ij}^{diff} which depend on the mechanism of the gaseous reagent solubility in the electrolyte and on the geometry of reagent transport through the electrolyte. For example, in the case of a thin film model of the microscopic process with planar diffusion and physical solubility of the reagent 'k'

$$i_k^{lim} = \frac{nFD_k H_k p_k}{\delta v_k} \tag{21}$$

Therefore, in accordance with Equation 16, $a_{jk}^{dif} = 0$ at $j \neq k$ and $a_{kk}^{dif} = 1$. The values of a_{jk}^{dif} not equal to zero at $j \neq k$ can be obtained in cases of chemical reagent solubility.

Recent experimental results concerning oxygen solubility in the 62% Li_2CO_3 + 38% K_2CO_3 electrolyte [16] indicate that chemical oxygen solubility with superoxide ion O_2^- formation

$$\tfrac{3}{4}O_2 + \tfrac{1}{2}CO_3^{2-} \rightleftharpoons O_2^- + \tfrac{1}{2}CO_2 \tag{22}$$

predominates over O_2^{2-} ion formation and physical solubility of oxygen. Assuming that the O_2^- ion is the basic (apart from CO_2) substrate of the cathodic electrochemical reaction, and that CO_2 solubility can be described using Henry's law, one obtains from Equation 16: $a^{\text{diff}}_{O_2,O_2} = 0.75$, $a^{\text{dif}}_{CO_2,O_2} = -0.5$, $a^{\text{dif}}_{CO_2,CO_2} = 1$, $a^{\text{dif}}_{O_2,CO_2} = 0$. Additionally, due to the small oxygen solubility in comparison with the CO_2 solubility one can write

$$Z^{\text{dif}}_{O_2} \gg Z^{\text{dif}}_{CO_2} \tag{23}$$

Denoting

$$s = Z^{\text{dif}}_{O_2}/Z^{\text{act}} \tag{24}$$

then one can obtain, by means of Equations 18, 20 and 23, the following inequalities

$$\frac{0.25a_{O_2} + 0.375s}{1 + s} \leqslant a^{\text{eff}}_{O_2} \leqslant \frac{a_{O_2} + 0.75s}{1 + s} \tag{25}$$

$$\frac{0.5a_{CO_2} - 0.25s}{1 + s} \leqslant a^{\text{eff}}_{CO_2} \leqslant \frac{a_{CO_2} - 0.5s}{1 + s} \tag{26}$$

On the other hand, experimental results obtained on the porous NiO cathode by Winnick and Ross [9]: $a^{\text{eff}}_{O_2} = 0.5$, $a^{\text{eff}}_{CO_2} = 0$ and by Tang *et al.* [10]: $a^{\text{eff}}_{O_2} = 0.3$, $a^{\text{eff}}_{CO_2} = 0$, permit us to write the set of inequalities on the grounds of Inequalities 25 and 26. Solution of this set of inequalities in the (s, a_{O_2}) and (s, a_{CO_2}) coordinate systems yields possible values of a_{O_2} and a_{CO_2} for the given s and, thereby, information about possible reaction mechanisms may be obtained.

Table 2. Alternative reaction mechanisms and related data for the NiO and Au cathodes in molten carbonates

Reaction	*Mechanism*	$i_0 \sim (p_{O_2})^{a_{O_2}}(p_{CO_2})^{a_{CO_2}}$		α_c	α_a	*Cathode material*	*Ref.*
		a_{O_2}	a_{CO_2}				
(27)	$\frac{1}{2}O_2 + CO_3^{2-} \rightleftharpoons O_2^{2-} + CO_2$ (bulk) $O_2^{2-} + e \rightleftharpoons [O^{2-}] + [O^-]$ (RDS) $[O^-] + e \rightleftharpoons [O^{2-}]$ $[O^{2-}] + CO_2 \rightleftharpoons CO_3^{2-}$	0.375	−1.25	0.5	1.5	Au	[7, 8]
(28)	$\frac{3}{4}O_2 + \frac{1}{2}CO_3^{2-} \rightleftharpoons O_2^- + \frac{1}{2}CO_2$ (bulk) $O_2^- + e \rightleftharpoons [O_2^{2-}]$ (RDS) $[O_2^{2-}] + e \rightleftharpoons [O^{2-}] + [O^-]$ $[O^-] + e \rightleftharpoons [O^{2-}]$ $[O^{2-}] + CO_2 \rightleftharpoons CO_3^{2-}$	0.625	−0.75	0.5	2.5	Au	[7, 8]
(29)	$\frac{3}{4}O_2 + \frac{1}{2}CO_3^{2-} \rightleftharpoons O_2^- + \frac{1}{2}CO_2$ (bulk) $O_2^- + e \rightleftharpoons 2[O^-]$ $[O^-] + CO_2 \rightleftharpoons [CO_3^-]$ (RDS) $[CO_3^-] + e \rightleftharpoons CO_3^{2-}$	0.25	0.50	1.0	1.0	NiO	[5]
(30)	$\frac{3}{4}O_2 + \frac{1}{2}CO_3^{2-} \rightleftharpoons O_2^- + \frac{1}{2}CO_2$ (bulk) $O_2^- + e \rightleftharpoons [O_2^{2-}]$ $[O_2^{2-}] + CO_2 \rightleftharpoons [CO_3^-] + [O^-]$ (RDS) $[O^-] + CO_2 \rightleftharpoons [CO_3^-]$ $[CO_3^-] + e \rightleftharpoons CO_3^{2-}$	0.50	0	1.0	2.0	NiO	Present paper

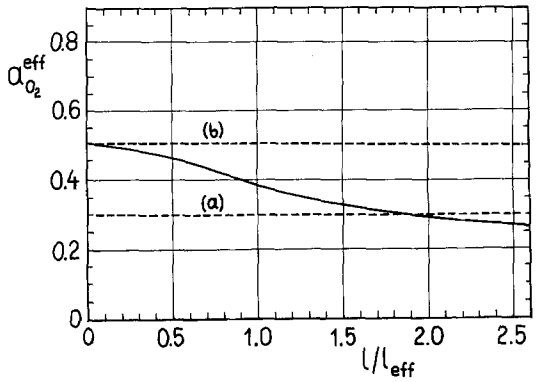

Fig. 1. Orders of the effective exchange currents. Continuous line, theoretical orders computed on the basis of Mechanism 30; broken lines, experimental data. (a) Tang *et al.* [10], (b) Winnick and Ross [9] (l_{eff} in both cases unknown).

2.3. *Cathodic reaction mechanism*

From among the reaction mechanisms considered, only two fulfil the above conditions (see Table 2): the reaction mechanism of Wilemski and Gelb [5] (at $s = 1$) and the reaction mechanism proposed (at $s = 0$). In the case of a thin film model of the microscopic process, Mechanism 30 seems to be more suitable. It results from the fact that the condition $s = 1$ ($Z_{O_2}^{dif} = Z^{act}$) requires the existence of an electrolyte film of about a few micrometres thickness. Mechanism 30 was used in further considerations. For this mechanism one can obtain for the generalized Butler–Volmer type equation:

$$i_c = -i_0^0 (p_{O_2})^{0.5} \left[\left(\frac{c_{O_2} c_{CO_2}}{c_{O_2}^0 c_{CO_2}^0} \right) \exp\left(\frac{-F\eta}{RT} \right) - \left(\frac{c_{CO_2}}{c_{CO_2}^0} \right)^{-1} \exp\left(\frac{2F\eta}{RT} \right) \right] \tag{31}$$

Orders of the effective exchange current as a function of the basic macroscopic parameter l/l_{eff}, calculated using Equations 17–19, are presented in Fig. 1 for oxygen with the proposed mechanism. From Fig. 1 one may conclude that the cathode of Winnick and Ross [9] was operating in the region of negligible ohmic loses ($l/l_{eff} = 0$) as opposed to that of Tang *et al.* [10].

2.4. *Gas phase transport description*

The multicomponent transport of gaseous reagents in the porous electrode has been described using the dusty gas model equations [17, 18]

$$-\frac{1}{RT} \operatorname{grad} p_i + \frac{B_0 p_i}{\mu D_{K,i}^{eff}} \operatorname{grad} p = \sum_{j=1}^{N} \frac{p_j N_i - p_i N_j}{p D_{ij}^{eff}} + \frac{N_i}{D_{K,i}^{eff}} \tag{32}$$

where

$$D_{ij}^{eff} = K_0 D_{ij} \tag{33}$$

$$B_0 = K_0 r_e^2 / 8 \tag{34}$$

It is important to mention that the coefficient K_0 depends on the void fraction of the electrolyte within the electrode, the so-called 'liquid porosity'. It may be estimated approximately as

$$K_0 = \frac{\varepsilon - \varepsilon_l - \varepsilon_d}{\tau} \tag{35}$$

where ε_l is the 'liquid porosity' and ε_d is the porosity connected with 'dead end' pores. For real porous structures factor τ varies within the interval $3 < \tau < 7$ [19].

For typical NiO porous cathodes

$$D_{K,i} \gg D_{ij} \tag{36}$$

and Knudsen diffusion is not taken into account. After some rearrangements one can transform the dusty gas model equations into a form more convenient for calculation:

$$\frac{dp_i}{dx} = -RT\left[\sum_{j\neq i}\frac{p_j N_i - p_i N_j}{pD_{ij}^{eff}} + \frac{\mu p_i M_i^{0.5}}{B_0}\frac{\Sigma_j N_j M_j^{0.5}}{(\Sigma_j p_j M_j^{0.5})^2}\right] \quad i = 1, \ldots, N \tag{37}$$

$$\frac{dp}{dx} = -\frac{\mu RT \Sigma_j N_j M_j^{0.5}}{B_0 \Sigma_j p_j M_j^{0.5}} \tag{38}$$

with the boundary conditions

$$p_i(x = 0) = p_i^0 \qquad i = 1, \ldots, N \tag{39}$$

$$N_i(x = l) = 0 \qquad i = 1, \ldots, N \tag{40}$$

Molar fluxes, N_j, are interconnected by equations of flux generation

$$n_j F\frac{dN_j}{dx} = -Si(\eta) \qquad j = 1, \ldots, N \tag{41}$$

Therefore, applying boundary conditions (40) one can find

$$n_i N_i(x) = n_j N_j(x) \qquad i, j = 1, \ldots, N \tag{42}$$

The set of differential equations (41) can be solved analytically using Equations 40 and 42

$$N_{O_2}(x) = \frac{j_T - j(x)}{4F} \tag{43}$$

$$N_{CO_2}(x) = 2N_{O_2}(x) \tag{44}$$

$$N_{N_2}(x) = 0 \tag{45}$$

where

$$j(x) = S\int_0^x i[p_1(x), \ldots, p_N(x)]dx \tag{46}$$

We define the concentration overpotential in the gas phase (the so-called 'Nernst loss') as the difference between the actual equilibrium potential of the electrode and the potential that would exist with the concentrations present under load [12]

$$\eta_N = -\frac{RT}{nF}\ln\frac{(p_{O_2}^0)^{0.5}p_{CO_2}^0}{(p_{O_2}(x))^{0.5}p_{CO_2}(x)} \tag{47}$$

Of course, at any point of the electrode

$$\eta_m = \eta(x) + \eta_N(x) + \Delta V_{IR}(x) \tag{48}$$

The system of differential and algebraic equations 2–4, 31, 37–40 and 43–48 gives us the full description of the porous MCFC cathode from the point of view of the model considered.

3. Results

The model equations with relative boundary conditions were solved numerically. Binary diffusion coefficients D_{ij} were calculated using Fuller, Schettler and Gidding's semi-empirical rule [20]. To calculate the gas mixture viscosity, the Sutherland constants were determined on the basis of the experimental results obtained for single gases [21]. Using the same Sutherland equation, the single

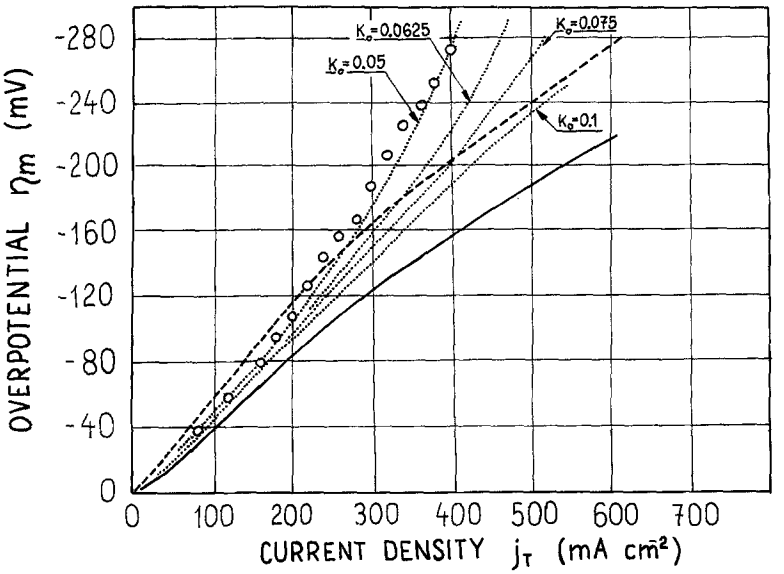

Fig. 2. Cathodic polarization curves computed on the basis of the proposed model at different K_0 parameters (dotted lines) and without gaseous phase transport limitations (continuous line), compared with Wilemski's model computations (broken line) [4] and with the IGT experimental data [23]. All the curves correspond to the gas composition A, i.e. $p_{O_2} = 0.10$ atm, $p_{CO_2} = 0.05$ atm, $p_{N_2} = 0.85$ atm.

gas viscosities were then estimated at the desired temperature, and lastly the gas mixture viscosity was calculated using Wilke's approximation [22]. All calculations were carried out at 923 K and $p = 1$ atm for the 62% Li_2CO_3 + 38% K_2CO_3 electrolyte. The standard current density i_0^0 (1.6 mA cm^{-2}) was estimated using the effective exchange current and total internal surface of the porous electrode which were experimentally determined by Winnick and Ross [9] for the NiO porous cathode (operated in the region of small ohmic losses).

The experimental polarization curves (total current density versus measured overpotential) published by the Institute of Gas Technology (IGT) [23] were firstly used to verify the NiO porous cathode model. The theoretical polarization curve at $p_{O_2} = 0.33$ atm and $p_{CO_2} = 0.67$ atm (for this composition there are practically no gaseous phase transport limitations) was adjusted to the experimental curve by using two adjustable parameters: $S(3600\,\text{cm}^{-1})$ and $\delta(0.5\,\mu\text{m})$. The individual adjustments were not made for any other IGT curves.

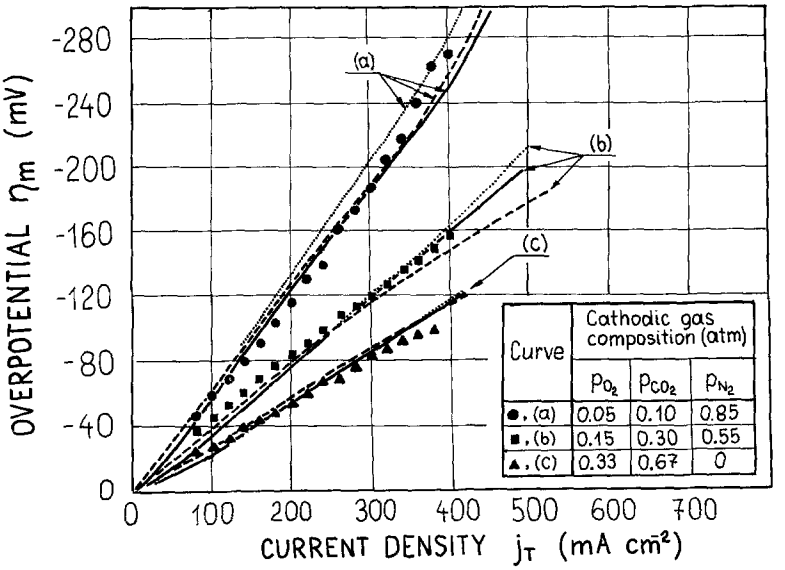

Curve	Cathodic gas composition (atm)		
	P_{O_2}	P_{CO_2}	P_{N_2}
●, (a)	0.05	0.10	0.85
■, (b)	0.15	0.30	0.55
▲, (c)	0.33	0.67	0

Fig. 3. Cathodic polarization curves computed on the basis of the proposed model at different K_0 parameters (dotted lines) and without gaseous phase transport limitations (continuous lines), compared with Wilemski's model computations (broken line) [4] and with the IGT experimental data [23] at different gas compositions.

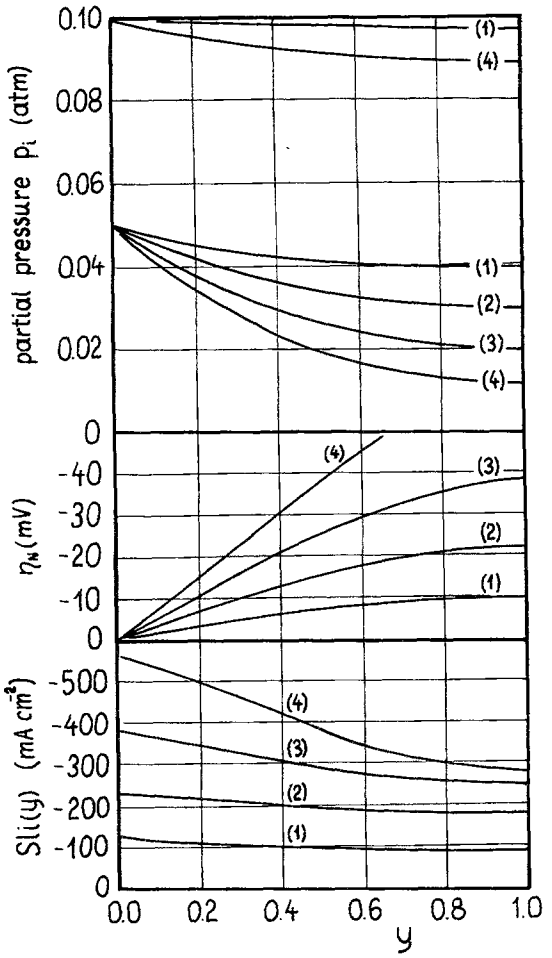

Fig. 4. Computed distributions of local O_2 and CO_2 partial pressures, Nernst losses and generated currents inside the porous NiO cathode at gas composition A, i.e. $p_{O_2} = 0.10\,\text{atm}$, $p_{CO_2} = 0.5\,\text{atm}$, $p_{N_2} = 0.85\,\text{atm}$. Total current densities: (1) $100\,\text{mA cm}^{-2}$; (2) $200\,\text{mA cm}^{-2}$; (3) $300\,\text{mA cm}^{-2}$; (4) $400\,\text{mA cm}^{-2}$.

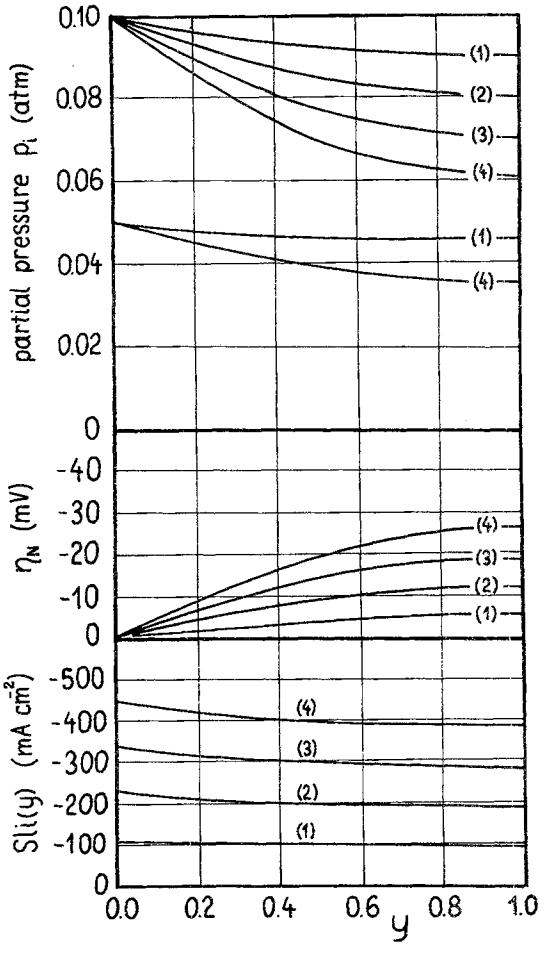

Fig. 5. Computed distributions of local O_2 and CO_2 partial pressures, Nernst losses and generated currents inside the porous NiO cathodes at gas composition B, i.e. $p_{O_2} = 0.05\,\text{atm}$, $p_{CO_2} = 0.10\,\text{atm}$, $p_{N_2} = 0.85\,\text{atm}$. Total current densities: (1) $100\,\text{mA cm}^{-2}$; (2) $200\,\text{mA cm}^{-2}$; (3) $300\,\text{mA cm}^{-2}$; (4) $400\,\text{mA cm}^{-2}$.

The results of computations for the polarization curves are compared in Figs 2 and 3 with the IGT experimental results and with the results of the thin film anisotropic model by Wilemski [4]. The comparison was performed at four different gas compositions and at different K_0 parameters. As shown in the figures, a satisfactory agreement with the IGT data was obtained at $K_0 = 0.05$. This result indicates a high degree of filling of the porous cathode with electrolyte (see Equation 35).

The experimentally observed 'inversion effect' at the gas compositions: (A) $p_{O_2} = 0.10\,\text{atm}$, $p_{CO_2} = 0.05\,\text{atm}$, $p_{N_2} = 0.85\,\text{atm}$; (B) $p_{O_2} = 0.05\,\text{atm}$, $p_{CO_2} = 0.10\,\text{atm}$, $p_{N_2} = 0.85\,\text{atm}$, could be explained by the present model. This effect is expressed by the comparable current densities at both A and B gas compositions in spite of a greater exchange current in the case of the composition A. This results from the greater gas phase transport limitations at the gas composition A, which implies relatively smaller local partial pressures of the electrochemically active species. The distributions of the local partial pressures $p_{O_2}(x)$, $p_{CO_2}(x)$, the Nernst losses $\eta_N(x)$, and the locally generated current densities within the porous cathode $i(x)Sl$ as a function of dimensionless coordinate $y = x/l$, ($l = 0.05\,\text{cm}$) are shown in Figs 4 and 5 for both A and B gas compositions.

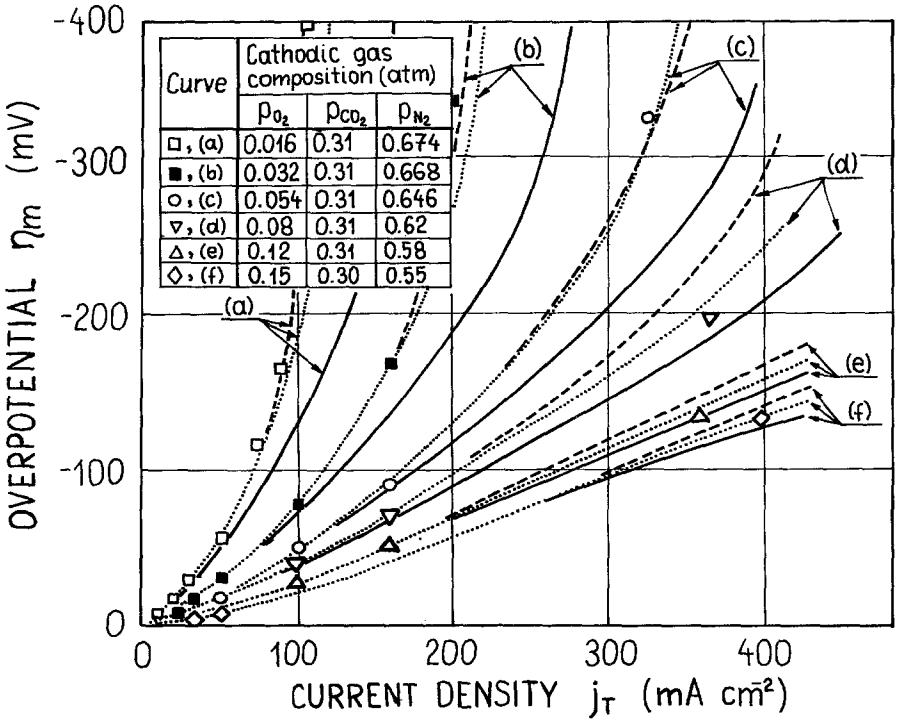

Fig. 6. Cathodic polarization curves computed on the basis of the proposed model without (continuous lines) and with (dotted lines) gaseous phase transport limitations ($K_0 = 0.05$), compared with experimental data and agglomerate model from [6] (broken line).

Modelling studies show that molecular diffusion predominates in the gas transport in the typical porous NiO cathode. The gas viscosity is of no practical importance in this case. The gaseous phase limitations are much greater at low partial pressures of the electrochemically active reagents (0.05–0.1 atm). At the same time, the relatively high carbon dioxide partial pressure is more important to prevent gas phase transport limitations. At greater partial pressures of the electrochemically active reagents, the gas phase transport limitation effects can be neglected in practice (e.g. at $j_T = 200\,\text{mA cm}^{-2}$ and $K_0 = 0.075$ the transport limitations are expressed by an increase of about 3% in the measured overpotential for the gas composition C: $p_{O_2} = 0.15\,\text{atm}$, $p_{CO_2} = 0.30\,\text{atm}$, $p_{N_2} = 0.55\,\text{atm}$).

Instead of S the same set of model parameters was taken to verify the model on the basis of the experimental results of Yuh and Selman [6]. From among different gas compositions, the gas composition C($p_{O_2} = 0.15\,\text{atm}$, $p_{CO_2} = 0.30\,\text{atm}$, $p_{N_2} = 0.55\,\text{atm}$) was applied in both IGT [23] and Yuh and Selman [6] experiments. Therefore electrochemically active specific internal suface of the cathode S_{YS} from [6] was calculated (assuming negligible ohmic losses) using a proportion

$$\frac{j^{\text{exp}}_{T,IGT}(\eta_m = 130\,\text{mV, gas C})}{j^{\text{exp}}_{T,YS}(\eta_m = 130\,\text{mV, gas C})} = \frac{S_{IGT}}{S_{YS}} \tag{49}$$

Cathodic polarization curves computed on the basis of the thin film isotropic model and agglomerate model [6] were compared with the experimental data from [6] in Fig. 6.

At oxygen partial pressures less than 0.03–0.04 atm, limiting currents due to the oxygen diffusion through the electrolyte are experimentally observed. Considerations of the isotropic model indicate that experimentally measured oxygen limiting current densities could be greatly influenced by the gas phase transport limitations. As was expected, limiting currents due to the carbon dioxide could be obtained for p_{CO_2} partial pressures less than 0.03–0.06 atm. The limiting currents depend mainly on the liquid porosity.

Acknowledgements

I would like to express my thanks to Professor L. Suski for suggestions during the preparation of this paper. This work has been sponsored by the Polish Research Project 03.10.6.

References

[1] J. Jewulski and L. Suski, *J. Appl. Electrochem.* **14** (1980) 135.
[2] Fuel Cell Research on Second Generation Molten Carbonate Systems, Vol. 1, Project 8984, Final Status Report, Insitute of Gas Technology, Chicago (1977).
[3] S. T. Szymański and H. R. Kunz, 'Molten Carbonate Cell Performance Model', Proceedings of the DOE/EPRI Workshop on Molten Carbonate Fuel Cells, Oak Ridge National Lab. (1979).
[4] G. Wilemski, *J. Electrochem. Soc.* **130** (1983) 117.
[5] G. Wilemski and A. Gelb, Paper presented at the Montreal Meeting of the ECS, May 9–14, Abstract 381 (1982).
[6] C. Y. Yuh and J. R. Selman, Paper presented at the Montreal Meeting of the ECS, May 9–14, Abstract 382 (1982).
[7] A. J. Appleby and S. Nicholson, *J. Electroanal. Chem.* **53** (1974) 105.
[8] *Idem, ibid.* **83** (1977) 309.
[9] J. Winnick and P. N. Ross, *J. Electrochem. Soc.* **128** (1981) 991.
[10] T. E. Tang, J. R. Selman, T. D. Claar and L. G. Marianowski, Extended Abstract 127, ECS Meeting, Fall, USA (1980).
[11] G. Wilemski, T. Wolf, D. Bloomfield, M. L. Finson, E. R. Pugh and K. L. Wray, Performance Model for the Molten Carbonate Fuel Cells, Final Report, PSI TR-190, Physical Sciences Inc., Woburn MA, USA (1979).
[12] J. L. Weaver and J. Winnick, *J. Electrochem. Soc.* **130** (1983) 20.
[13] A. C. Riddiford, *J. Chem. Soc.* (1960) 1175.
[14] L. J. Bregoli and H. R. Kunz, *J. Electrochem. Soc.* **129** (1982) 2711.
[15] Molten Carbonate Fuel Cell Large Stack Development, Project 200/ET-ENS/80, NYSERDA, New York (1980).
[16] S. W. Smith, W. M. Vogel and S. Kapelnaar, *J. Electrochem. Soc.* **129** (1982) 1668.
[17] E. A. Mason, A. P. Malinauskas and R. B. Evans, III, *J. Chem. Phys.* **46** (1967) 3199.
[18] R. Jackson, 'Transport in Porous Catalysts', Elsevier, Amsterdam (1977).
[19] C. N. Satterfield, 'Heterogeneous Catalysis in Practice', McGraw-Hill, New York (1982).
[20] E. N. Fuller, P. D. Schettler and J. C. Giddings, *Ind. Eng. Chem.* **58** (1966) 18.
[21] I. F. Golubiev, Vjaskost gazov i gazovykh smesej, GIFML, Moscow (1959).
[22] R. C. Reid, J. M. Prausnitz and T. K. Sherwood, 'The Properties of Gases and Liquids', McGraw-Hill, New York (1977).
[23] Fuel Cell Research on Second Generation Molten Carbonate Systems, Vol. II, Project 8984, Final Status Report, Institute of Gas Technology, Chicago (1977).